In-situ/operando X-ray absorption spectroscopic investigation of the electrode/electrolyte interface on the molecular scale

Li Cheng Kao[a,⊥], Xuefei Feng[a,b,⊥], Yang Ha[a], Feipeng Yang[a,b] ,Yi-Sheng Liu[a], Nathan T. Hahn[b,c], James MacDougall[d], Weilun Chao[d], Wanli Yang[a], Kevin R. Zavadil[b,c], Jinghua Guo[a,b,e] *

[a] Advanced Light Source, Lawrence Berkeley National Laboratory, Berkeley, California 94720, USA

[b] Joint Center for Energy Storage Research, Lemont, Illinois 60439, USA

[c] Material, Physical and Chemical Sciences, Sandia National Laboratories, Albuquerque, New Mexico 87185, USA.

[d] Center for X-ray Optics, Lawrence Berkeley National Laboratory, Berkeley, California 94720, USA

[e] Department of Chemistry and Biochemistry, University of California, Santa Cruz, California 95064, USA

Abstract

A method for performing X-ray absorption spectroscopy (XAS) in the soft X-ray region was developed to investigate the surface-sensitive electron signal of electrode/electrolyte interfaces in common multivalent based organic solvents under *in situ/operando* conditions. Our approach enables us to probe the molecular-scale structure of electrode interfaces by measuring total electron yield and is suitable for redox systems exhibiting low intrinsic electrochemical current. *In-situ* F K-edge XAS measurements in a 0.5 M Magnesium bis(trifluoromethanesulfonimide)/2-Methyltetrahydrofuran (Mg(TFSI)$_2$/2-MeTHF) electrolyte were carried out to determine the evolution of interfacial species during the electrochemical charging/discharging process. Time-dependent density-functional theory (TD-DFT) simulation indicate that the F K-edge evolution is the result of interfacial chemical environment change driven by electrochemical potential. In addition, we performed the "*operando* XAS" which runs the CV and collects spectra simultaneously. By using this method, the non-equilibrium state of condensed matter interfaces and interfacial dynamical transient process can be revealed.

Keywords: *In-situ/operando*, soft X-ray, XAS, interface, battery

1. Introduction

The last several decades have seen a renaissance of electrochemistry. An understanding and control of electrochemical processes are essential for the development of sustainable new battery systems to enable cost-effective energy storage [1-5]. As the promising candidate for the post-lithium-ion batteries, non-aqueous multivalent (e.g., Mg^{2+}, and Zn^{2+}) metal cells provide an attractive opportunity in energy storage devices because of higher theoretical volumetric capacity of a multivalent metal anode and the restricted dendrite formation on the surface of the anode [6-8]. The development of compatible multivalent electrolytes with a metal anode and reversible multivalent intercalation cathodes is a significant challenge requiring extensive investigation on fundamental understanding of electrolyte and electrode properties and behavior [9, 10].

In the battery systems, the interactions at the electrode/electrolyte interfaces which dictate the battery performance are at the heart of innovation. Understanding what surface structures form while operating the electrochemical cell at certain bias is of particular interest. The electrochemical cell stability is largely an interfacial phenomenon whose description requires an accurate dealing with issues of oxidation/reduction potentials [11-15], the explanation for the charge redistributions [16, 17], and modeling of voltage-dependent of the chemical reactions, and the related transition pathways [18, 19]. In comparison to simple cations solvation evident in aqueous solutions, complex multivalent based organic salts demonstrate a considerable degree of contact-ion pairing in common organic solvents even at relatively low concentrations [20-23]. In addition, these condensed matter interfaces are only to a limited extent approachable to experimental surface analytic methods, especially under operating electrochemical conditions.

Recent technological advances have made it possible to extend powerful microscopy and spectroscopy to characterize the molecular-scale structure of electrode interfaces. Transmission electron microscopy [24], X-ray photoelectron spectroscopy [25-27], and X-ray absorption spectroscopy (XAS) [28-32], from vacuum to ambient environments and operating with electrochemical potential control, provide new opportunities for *in-situ* investigation of electrode/electrolyte interfaces. XAS, which is sensitive to the local structure and chemical environment, is element-specific and provides information regarding the electronic structure of the excited atom. Previous studies using *in-situ* XAS to characterize battery electrodes were limited to acquisition of the photon signal, which probes micrometers of depth, masking the relevant interfacial information [28, 31, 33]. Collection of the surface-sensitive electron signal for an *in-situ* liquid electrochemical cell has only been demonstrated using x-ray source intensity modulation for aqueous electrolytes [29,

30]. For instance, Velasco-Velez *et al.* probed the water interfacial reaction on the gold electrode [29] and Wu *et al.* discovered the molecular structure evolution of aqueous sulfuric acid on platinum electrode [30]. In addition, Schön *et al.*, demonstrated that XA spectra can also be obtained without modulation of the X-ray beam, termed as total ion yield (TIY) [34]. However, the electronic structure of electrified solid–liquid interfaces was acquired at several selected potentials. Hence, it is eager to develop a method which can truly investigate the dynamic interfacial molecular structure of electrode/electrolyte, for instance, the electrode/electrolyte interaction in the battery system.

We further advance the *in-situ* XAS technique by demonstrating methods for acquisition of the surface-sensitive electron signal while controlling electrode potential. Moreover, we conduct the real "*operando* XAS" experiment in which spectral data is acquired simultaneously with the voltammetric response of the electrode interface, revealing transient interfacial processes. Notable is the ability to dynamically record interfacial reactions probing the non-equilibrium state of the electrode interface through XAS measurement.

2. Experimental

2.1 Beamlines

In-situ/operando synchrotron-based XAS experiments were conducted on the beamlines 8.0.1 and 7.3.1 of Advanced Light Source (ALS) at Lawrence Berkeley National Laboratory. In this facility, the undulator (U5) beamline 8.0.1 has a spherical grating monochromator provide a linearly polarized photon beam with an energy range from 80 eV to 1250 eV and a resolving power up to 5000, and bending magnet beamline 7.3.1 provide a linearly polarized photon beam with an energy range from 250 eV to 1400 eV and a resolving power up to 3000. XAS spectra were collected by measuring the total electron yield (TEY) and the total fluorescent yield (TFY) simultaneously in each experiment. TFY is a bulk-sensitive technique because the mean free path of photons is in the micrometer range. In contrast, TEY is a surface-sensitive technique because the electron penetration depth from the working electrode (e.g. the interface of interest) is limited within a few nanometers. All XAS spectra have been normalized by the incident beam, which is measured by a clean gold mesh.

2.2 Electrolytes

All chemical preparations were performed in an Ar glovebox (Mbraun, H_2O < 5 ppm, and O_2 < 3 ppm) at room temperature. Prior to the electrolyte preparation, $Mg(TFSI)_2$ ($C_4F_{12}MgN_2O_8S_4$, 97%, TCI) and $Zn(TFSI)_2$ ($C_4F_{12}ZnN_2O_8S_4$, Solvionic, 99.5%) were dried under vacuum for 12 h at 150 and 120 °C, respectively. Predetermined amounts

of $Mg(TFSI)_2$ and $Zn(TFSI)_2$ were added to 2-MeTHF (Merck, >98%) and stirred overnight. The solutions were then set aside for further utilization.

2.3 *In-situ/operando* electrochemical system

The static liquid electrochemical cell was operated inside the main chamber of the wet-RIXS endstation of the beamline 8.0.1 and 7.3.1 at a background pressure of ~10^{-9} mbar. Fig. 1a shows a side view of the cell. The structure of the cell has been reported in our previous study. [30] Briefly, 50 μL liquid is loaded in a polyether ether ketone (PEEK) based holder and sealed using an ultrathin x-ray transparent Au coated Si_3N_4 membrane and a perfluoro elastomer O-ring. The membrane serves as a working electrode (WE) for which potential is controlled either in a two electrode *in-situ* or a three electrode *operando* configuration. *In-situ* measurements employed a Pt wire counter electrode (CE) and cell potentials were applied with the offset bias control of a low noise current preamplifier (SR570, Stanford Research Systems) used to measure the x-ray induced electron signal. *Operando* measurements were made with a potentiostat (Biologic SP-200, Seyssinet-Pariset) using either Mg or Zn wire counter electrodes (CE), depending on the electrolyte under study, with a Pt wire quasi-reference electrode (qRE).
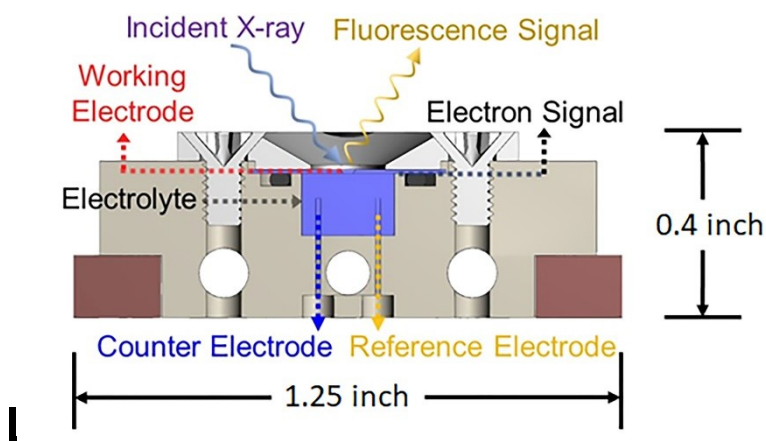

Fig. 1. A schematic diagram of the electrochemical cell. In this study, Au coated Si_3N_4 window, Pt wire and Zn(Mg) wire are used as working (WE), reference (RE) and counter (CE) electrodes, respectively. Both TEY and TFY signals were collected.

2.4 TD-DFT simulation of F K-edge XAS

DFT Calculations were carried out using the package ORCA 4.0.1 on the high performance supercomputing cluster Lawrencium at the Lawrence Berkeley Lab. The initial structures were built from scratch and then geometry optimized [35]. TD-DFT calculations were completed on the optimized structures to model XANES spectra

using the transitions from the F 1s to probable unoccupied orbitals [36]. All the calculations were done using the B3LYP functional [37], def2-TZVP basis set [38], SARC/J auxiliary basis set [39], with ZORA [39] in THF solutions using the PCM model [40, 41].

3. Results and discussion

3.1. *In-situ* studies

To investigate the electrode/electrolyte interface under reaction conditions, a surface sensitive TEY signal without substantial interference from the bulk electrolyte is critical for the electrochemical system. In contrast to dominant intrinsic electrochemical current, the incident x-ray induced TEY signal is relatively low and hard to separate from the intrinsic signal. It should be mentioned that although there are techniques to detect a weak electron signal at the interface, the background noise level may increase as multiple electronic devices are introduced into the data collecting system. Additionally, for a battery system which acts as a capacitor, the periodic photon current will influence the stability of the electrolyte/electrode interface and the spectra may change accordingly since it is sensitive to the interfacial electronic structure. Thus, it is important to set up the system correctly for different *in-situ/operando* studies. To minimize the influence on the stability of the electrolyte/electrode interface, a different set-up, i.e. normal mode, was used to collect the TEY signal. The time-resolved F K-edge TEY signal from the electrochemical static liquid cell with 0.5 M $Mg(TFSI)_2$/2-MeTHF at open-circuit potential (OCP) with x-ray illumination was plotted in Fig. 2a. The spectra were recorded continuously and each spectrum took about 400 seconds, and the inverted intensity was caused by the opposite electron refilling direction. As a function of time, the TEY signal slowly decayed, eventually showing lower background currents and the F featured peaks at 688-694 eV. Although the main feature of the F K-edge in Fig. 2a was broad and not clear enough to distinguish each peak, this set-up to probe the interface-sensitive TEY is still very promising after background subtraction and normalization.
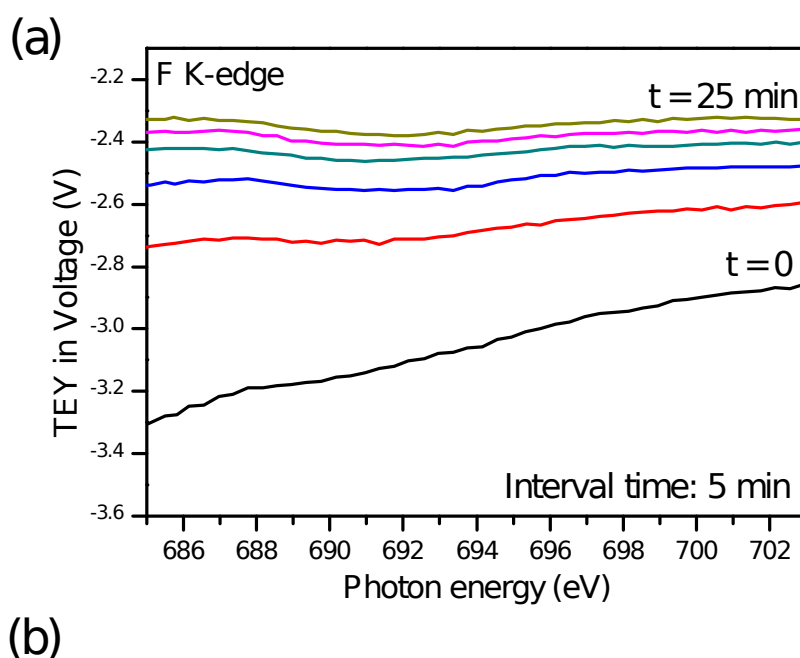
Fig. 2. (a) The time-resolved F K-edge TEY signal of 0.5 M Mg(TFSI)$_2$/2-MeTHF at OCP with X-ray illumination. The spectra were taken continuously and the interval time between each spectrum is 5 minutes. (b) Sample currents of 0.5 M Mg(TFSI)$_2$/2-MeTHF at different potentials without X-ray illumination. It takes about 0.5 ~ 1 h to reach the equilibrium state.

To provide a systematic understanding of the *in-situ* set-up to collect the interface sensitive TEY, the faradic and background current generation mechanism should be clarified. Sample currents of electrochemical static liquid cell (0.5 M Mg(TFSI)$_2$/2-MeTHF) implemented at different potentials without X-ray illumination are shown in Fig.2b. Once the current circuit formed, the sample current started to decay and then became stable. The larger the bias applied, the longer the time required to stabilize the faradic and background currents. The process of approaching the current steady state

can infer from the discharging of the whole system and the rearrangement of ions in electrolyte. When the higher the bias is applied, the longer the time is required to stabilize. It is notable that the decaying sample currents are correlated with the curve shape. To obtain the reduced TEY spectra, subtracting the faradic and non-faradaic background current before normalization is essential.

After removal of the background current, the main feature of F K-edge of 0.5 M Mg(TFSI)$_2$/2-MeTHF operating at several chosen potentials in TEY mode is depicted in Fig. 3a. These spectra are quite different from the initial, as equilibrated OCP to -1.95 V (vs. Pt) and they show substantial variations as a function of the decreasing electrode potential. These spectra can be divided into two regions. The first region contains a narrow peak A, located below the F K-edge absorption threshold (~690 eV) [42]. The second region is dominated by the broader absorption bands B that are located near the absorption threshold (~694 eV) [43]. A similar F K-edge TEY spectra is measured for 0.5 M Zn(TFSI)$_2$/2-MeTHF at equilibrium as shown in Fig. 3b, indicating that TFSI- assumes a similar interfacial conformation at an equilibrated Au interface with both electrolytes. The peaks labeled as A and B can be assigned to the F 1s electron transitions to π* (C-F) and σ* (C-F) unoccupied molecular orbitals, respectively [43, 44]. Detailed TD-DFT simulation results are described in section 3.2.

Considering the shallow probe depth for the TEY mode, we observe spectral changes related to electrolyte decomposition that yield surface film formation for the Mg(TFSI)$_2$ electrolyte. The TEY data of Figure 3a show the dominant intensity shifts from peak A to B with increased reductive polarization toward -1.95 V vs. Pt, just above the onset for Mg metal deposition. When the potential is returned to open circuit (0 V vs. Pt), the TEY spectrum is unchanged indicating an irreversible change has taken place in the F molecular identity and/or environment. Reference voltammetry of this electrolyte yields cathodic current signaling electrolyte decomposition with the earliest change in TEY line shape (-1 V vs Pt). In contrast to this change in TEY response, the TFY spectra in Fig. 3b exhibit no change in line shape over this potential range, demonstrating that TFSI anion decomposition is restricted to the electrode surface. These F K-edge TFY spectra are similar to those of previous reports where the main edge measured at 692 eV is attributed to the −CF$_3$ group of TFSI$^-$ [42]. Note that in this system, the probing depth of TEY mode is about 1~2 nm while it's over 100 nm for TFY mode, the spectra comparison in TEY and TFY modes indicates the significant difference of the interface and bulk evolutions at different potentials. This contrast in electron and fluorescent yield measurements highlight TEY as a crucial technique to understand the molecular-scale structure of electrode-electrolyte interfaces.

Such electrode/electrolyte interfacial reactions can be studied systematically across electrolyte type through replacement of cation, anion or solvent. We show an example of replacing Mg with Zn to determine the extent to which a decomposition reaction impacts Zn electrodeposition. The data of Fig. 3c, d similar equilibrium (open circuit) TEY and TFY spectra as Mg as expected for two divalent cations of similar charge radius. Where a similar loss in peak A relative to B TEY intensity is observed for a small anodic polarization of +0.17 V vs. Pt, subsequent cathodic polarization restores the original line shape with no discernable change in the bulk TFSI⁻ spectra (TFY). We propose anodic decomposition of the electrolyte involving the anion result is reversible adsorption of a F containing product that does not affect subsequent Zn electrodeposition on or alloying with the Au WE. Further study need to be carried out in the future to understand the difference between $Mg(TFSI)_2$ and $Zn(TFSI)_2$ based system.
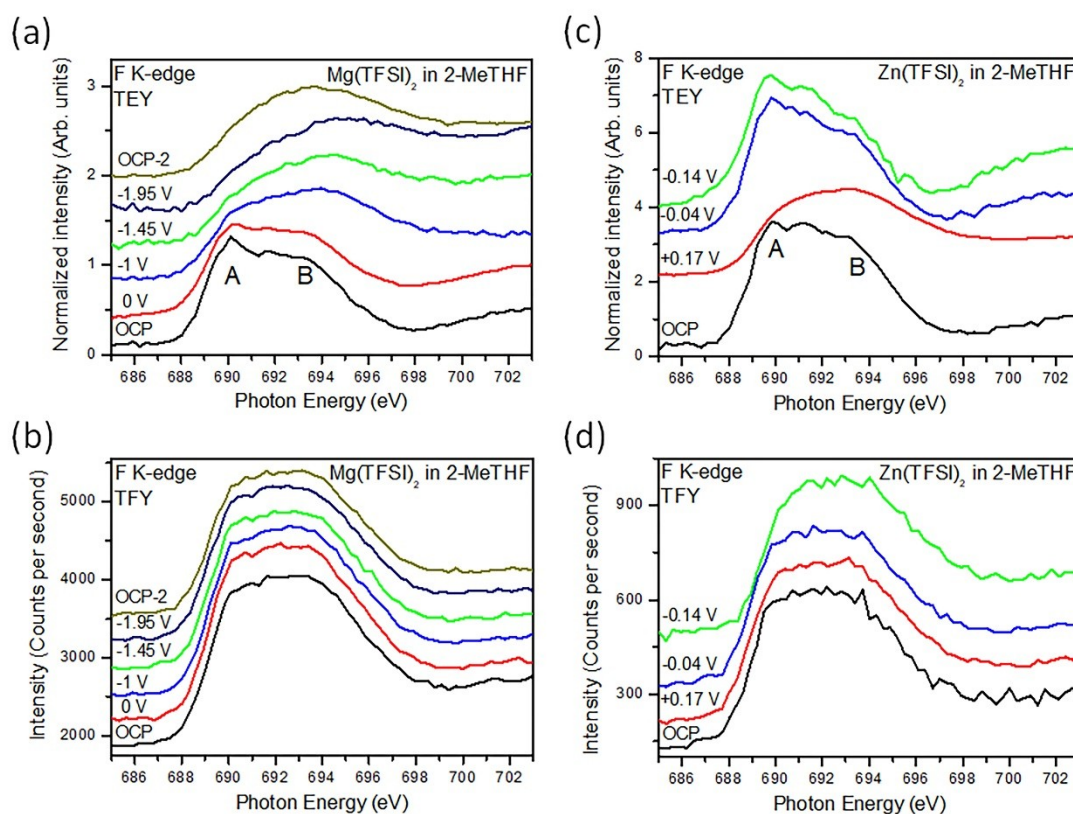

Fig. 3. (a, c) TEY and (b, d) TFY of F K-edge XAS in 0.5 M $Mg(TFSI)_2$/2-MeTHF and $Zn(TFSI)_2$/2-MeTHF, respectively. The ratio of the peak A and B variation as a function of applied potential (vs. Pt) in both electrolytes has been observed.

3.2 DFT Calculation and possible interfacial species

The geometry optimized structures of the TFSI⁻ with and without the Mg^{2+} counter ion are shown in Fig.4. It should be noted that without the counter ion, the TFSI⁻ tend

to have the bulky groups stay apart to minimize the total steric effect. When the counter ion is present, the TFSI⁻ tend to have all the negatively charged groups wrapped around the positively charged counter ion. Such changes in the molecular structure and chemical environment are reflected in the simulated spectra (Fig. 4). The lower energy peak at 691 eV, which is assigned as the F 1s to the C-F π^* transitions, representing more delocalize oribtalsare more delocalized. This assignment is consistent with experimental findings that at reducing voltage, most of the Mg^{2+} ions undergo decomposition from the gold surface, thus most of the TFSI⁻ in the solvent are in free form. In addition, the contribution of the π^*(C-F) peak was largest at nearly perpendicular orientation to the electrode, whereas the σ^* (C-F) at about 694 eV became prominent at grazing incidence. The relative intensity of π^* and σ^* transition can be interpreted as TFSI⁻ complex rotation while applying the bias and approaching to the electrode [23, 31, 45].
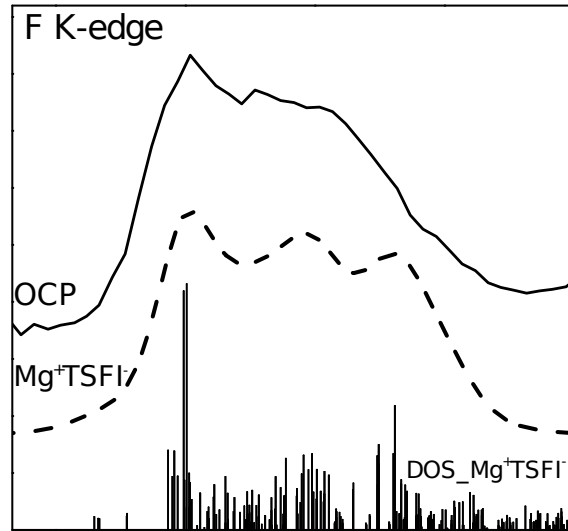
Fig. 4. The experimental (solid line) and simulated (dash line) F K-edge spectra of TFSI⁻ ions at initial equilibrium and at a reducing potential close to the deposition potential. The geometry optimized structure with and without Mg²⁺ counter ions are plotted next to the simulated spectra of possible interfacial species under different potentials. The corresponding density of unoccupied states at F K-edge are presented at the bottom shown in blue and black vertical bar, respectively.

3.3 *Operando* XAS measurements

As described above, we have performed *in-situ* XAS measurements on different systems at fixed potentials. These results can help to understand the evolution of electrolyte/electrode interface at equilibrium states. However, one may note that for real battery cycling, the electrolyte/electrode interfaces are always at non-equilibrium

states, which implies that the potential at the interface is actually not fixed. Thus, comparison of the two different type of interface is necessary for building the interface model correctly. To meet this aim, *operando* XAS is performed by connecting the three electrodes with a potentiostat which runs the CV when the electron signal generated by incident x-ray illumination was recorded simultaneously (Figure 5).
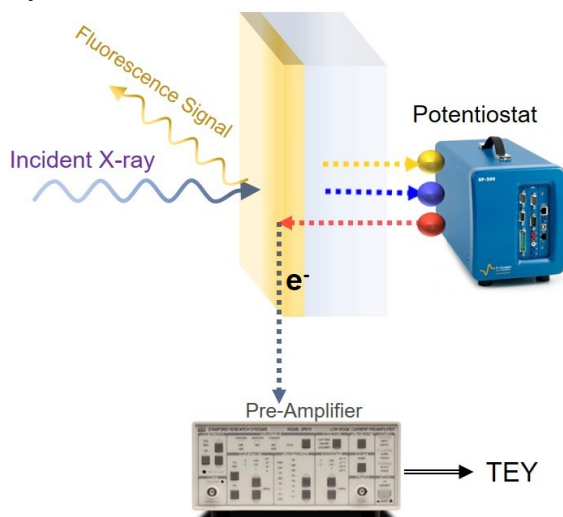

Fig. 5. *Operando* XAS experiment set-up. WE (red), RE (blue) and CE (yellow) are connected to potentiostat while the window is connected to pre-amplifier for XAS spectra collection during cell cycling.

We take 0.5 M Zn(TFSI)$_2$/2-MeTHF as an example and the *operando* F K-edge TEY-XAS together with CV to spectroscopically probe the non-equilibrium state of the electrode interface (Fig. 6a). The left panel of Fig. 6a shows the voltammetric response of an Au working electrode at room temperature at a scan rate of 6 mV/s versus a Zn wire reference electrode and a Pt counter electrode. A significant change of intensity ratio of peak A and B (around 691 eV and 694 eV) at 0 V and 1 V is observed while the intensity of these two peaks is unchanged throughout the remainder of the potential range. Additionally, we find the peak ratio of A and B are different at the same potentials in the potential step (Fig. 3c) and CV experiments (Fig. 4a), indicating that the interfacial chemical environment at equilibrium/non-equilibrium state are not the same. Moreover, after subtracting the background between 686 eV and 700 eV, the integrated areas of F K-edge TEY signal (area above the background) as a function of potential is presented in Fig. 6b. The evolution of intensity can be divided into three regions:(1) The region Ⅰ undergoes chemical decomposition involving either anions or solvent, which leads to irreversible reactions, electrolyte loss, and possible deposition of decomposition products on the electrode surface. The high concentration of TFSI$^-$ anions increases ion-pairing possibility, which in turn leads to a higher number of TFSI$^-$ anions being exposed to the transient

metal ion radical and subsequent decomposition. Region Ⅱ and Ⅲ can be assigned as double layer formation and pre-alloying reaction, respectively. On the basis of the *in-situ/operando* XAS measurements, the reductive decomposition of TFSI⁻ should occur at the potential of that in region Ⅰ. Although further experiments and computation need to be carried out to build a complete interfacial model describing the impact of electrochemical potential, we have demonstrated that *operando* XAS can be a promising tool to probe the physicochemical processes taking place in an active sensing element in real time and under operating conditions, offering insight into the electrochemically active species or deactivation mechanisms. The understanding of electrolyte/electrode interaction responsible for SEI effects will lead to increase stability of the electrolytes at high potential and thus to the development of better battery.
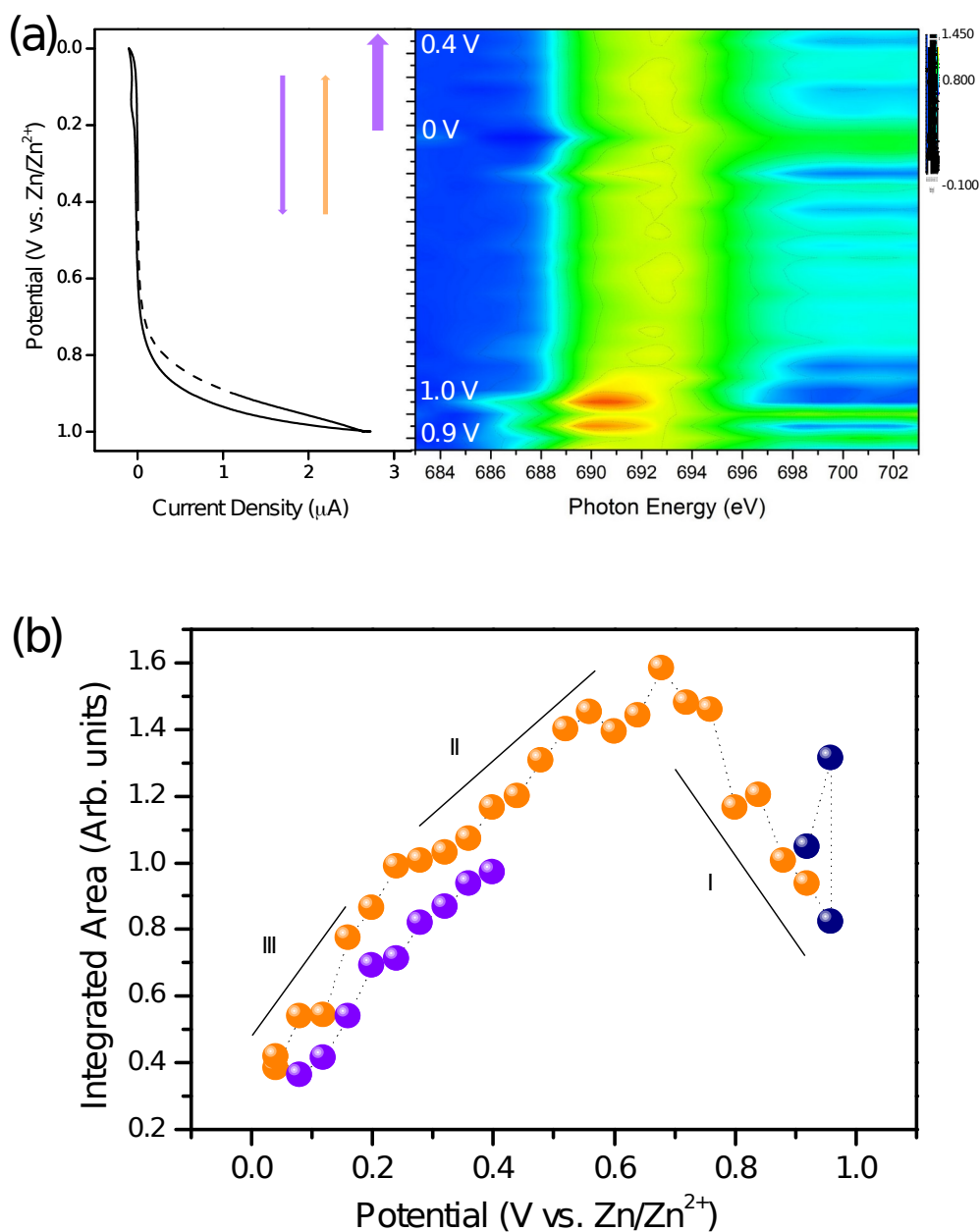
Fig. 6. (a) F K-edge TEY XAS map vs. potential between working electrode and reference electrode. 0.5 M Zn(TFSI)$_2$ in 2-MeTHF is used in this *operando* experiment. The *operando* XAS was collected in the solid line region. The F K-edge intensity change is shown in (b). The dark blue, orange and purple symbols are the integrated area of F K-edge in the different stages in (a).

4. Conclusions

In this work, an *in-situ/operando* XAS experimental method was established to study the electrode/electrolyte interface in non-aqueous solutions. The *in-situ* set-up is designed to obtain TEY signal from the interfaces in low intrinsic electrochemical-current systems. By using this method, the changes of F K-edge TEY main features

were observed in two different systems, indicating the evolution of interfacial species at different potentials. These results are also confirmed by TD-DFT simulation. For comparison, by collecting XAS spectra during CV cycling in 0.5 M $Zn(TFSI)_2$/2-MeTHF system, the interface transient process at non-equilibrium state is proposed. This underlying thermodynamic mechanism for interfacial species from the electrolyte to the electrode surface can be essential for a fundamental understanding of electrochemical reactions, with applications in the battery field.

References

[1] K. Xu, Nonaqueous liquid electrolytes for lithium-based rechargeable batteries, Chem. Rev. 104 (2004) 4303−4418, https://doi.org/10.1021/cr030203g.

[2] L. Ji, M. Rao, H, Zheng, L. Zhang, Y. Li, W. Duan, J. Guo, E. J. Cairns, Y. Zhang, Graphene oxide as a sulfur immobilizer in high performance lithium/sulfur cells, J. Am. Chem. Soc. 133 (2011) 18522-18525, https://doi.org/10.1021/ja206955k.

[3] K. Xu, Electrolytes and interphases in Li-ion batteries and beyond, Chem. Rev. 114 (2014) 11503−11618, https://doi.org/10.1021/cr500003w.

[4] A. Ponrouch, C. Frontera, F. Bardé, M. R. Palacín, Towards a calcium-based rechargeable battery, Nature Mater. 15 (2016) 169-172, https://doi.org/10.1038/nmat4462.

[5] O. M. Magnussen, A. Groß., Toward an atomic-scale understanding of electrochemical interface structure and dynamics, J. Am. Chem. Soc. 141 (2019) 4777-4790, https://doi.org/10.1021/jacs.8b13188.

[6] D. Aurbach; Z. Lu; A. Schechter; Y. Gofer, H. Gizbar, R. Turgeman, Y. Cohen, M. Moshkovich, E. Levi, Prototype systems for rechargeable magnesium batteries, Nature 407 (2000) 724-727, https://doi.org/10.1038/35037553.

[7] J. Muldoon, C. B. Bucur, A. G. Oliver, T. Sugimoto, M. Matsui, H. S. Kim, G. D. Allred, J. Zajicek, Y. Kotani, Electrolyte roadblocks to a magnesium rechargeable battery, Energy Environ. Sci. 5 (2012) 5941−5950,

https://doi.org/10.1039/C2EE03029B.

[8] J. Muldoon, C. B. Bucur, T. Gregory, Quest for nonaqueous multivalent secondary batteries: magnesium and beyond, Chem. Rev.114 (2014) 11683-11720, https://doi.org/10.1021/cr500049y.

[9] D. Y. Kim, Y. Lim, B. Roy, Y.-G. Ryu, S.-S. Lee, Operating mechanisms of electrolytes in magnesium ion batteries: chemical equilibrium, magnesium deposition, and electrolyte oxidation, Phys. Chem. Chem. Phys. 16 (2014) 25789–25798, https://doi.org/10.1039/C4CP01259C.

[10] E. M. Erickson, E. Markevich, G. Salitra, D. Sharon, D. Hirshberg, E. Llave, I. Shterenberg, A. Rosenman, A. Frimer, D. Aurbach, Development of advanced rechargeable batteries: a continuous challenge in the choice of suitable electrolyte solutions, J. Electrochem. Soc. 162 (2015) A2424–A2438, https://doi.org/10.1149/2.0051514jes.

[11] I. Rungger, X. Chen, U. Schwingenschlögl, S. Sanvito, Finite-bias electronic transport of molecules in a water solution, Phys. Rev. B 81 (2010) 235407, https://doi.org/10.1103/PhysRevB.81.235407.

[12] M. E. Björketun, Z. H. Zeng, R. Ahmed, V. Tripkovic, K. S. Thygesen, J. Rossmeisl, Avoiding pitfalls in the modeling of electrochemical interfaces, Chem. Phys. Lett. 555 (2013) 145– 148, https://doi.org/10.1016/j.cplett.2012.11.025.

[13] N. Kharche, J. T. Muckerman, M. S. Hybertsen, Ab initio electronic structure of liquid water, Phys. Rev. Lett. 113 (2015) 176802, https://doi.org/10.1103/PhysRevLett.117.186401.

[14] K. Leung, Predicting the voltage dependence of interfacial electrochemical processes at lithium-intercalated graphite edge planes, Phys. Chem. Chem. Phys. 17 (2015) 1637-1643, https://doi.org/10.1039/C4CP04494K.

[15] M. Nielsen, M. E. Björketun, M. H. Hansen, J. Rossmeisl, Towards first principles modeling of electrochemical electrode–electrolyte interfaces, Surf. Sci. 631 (2015) 2-7, https://doi.org/10.1016/j.susc.2014.08.018.

[16] R. Jinnouchi, A. B. Anderson, Electronic structure calculations of liquid-solid interfaces: Combination of density functional theory and modified Poisson-Boltzmann theory, Phys. Rev. B 77 (2008) 245417, https://doi.org/10.1103/PhysRevB.77.245417.

[17] K. Letchworth-Weaver, T. A. Arias, Joint density functional theory of the electrode-electrolyte interface: Application to fixed electrode potentials, interfacial capacitances, and potentials of zero charge, Phys. Rev. B 86 (2012) 075140, https://doi.org/10.1103/PhysRevB.86.075140.

[18] N. Bonnet, T. Morishita, O. Sugino, M. Otani, First-principles molecular dynamics at a constant electrode potential, Phys. Rev. Lett. 109 (2012) 266101,

https://doi.org/10.1103/PhysRevLett.109.266101.

[19] N. Bonnet, I. Dabo, N. Marzari, Chemisorbed molecules under potential bias: detailed insights from first-principles vibrational spectroscopies, Electrochimica. Acta 121 (2014) 210– 214, https://doi.org/10.1016/j.electacta.2013.12.115.

[20] R. Mohtadi, M. Matsui, T. S. Arthur, S.-J. Hwang, Magnesium borohydride: from hydrogen storage to magnesium battery, Angew. Chem., Int. Ed. 51 (2012) 9780– 9783, https://doi.org/10.1002/ange.201204913.

[21] S.-Y. Ha, Y.-W. Lee, S. W. Woo, B. Koo, J.-S. Kim, J. Cho, K. T. Lee, N.-S. Choi, Magnesium (II) bis (trifluoromethane sulfonyl) imide-based electrolytes with wide electrochemical windows for rechargeable magnesium batteries, ACS Appl. Mater. Interfaces 6 (2014) 4063-4073, https://doi.org/10.1021/am405619v.

[22] Y. Shao, N. N. Rajput, J. Hu, M. Hu, T. Liu, Z.Wei, M. Gu, X. Deng, S. Xu, K. S. Han, J. Wamg, Z. Nie, G. Li, K. R. Zavadil, J. Xiao, C. Wang, W. A. Henderson, J.-G. Zhang, Y. Wang, K. T. Mueller, K. Persson, J. Liu, Nanocomposite polymer electrolyte for rechargeable magnesium batteries, Nano Energy 12 (2015) 750– 759, https://doi.org/10.1016/j.nanoen.2014.12.028.

[23] N. N. Rajput, X. Qu, N. Sa, A. K. Burrell, K. A. Persson, The coupling between stability and ion pair formation in magnesium electrolytes from first-principles quantum mechanics and classical molecular dynamics, J. Am. Chem. Soc. 137 (2015) 3411-3420, https://doi.org/10.1021/jacs.5b01004.

[24] H. Zheng, Y. S. Meng, Y. Zhu, Frontiers of in situ electron microscopy, MRS Bull. 40 (2015) 12–18, https://doi.org/10.1557/mrs.2014.305.

[25] M. V. Lebedev, W. Calvet, T. Mayer and W. Jaegermann, Photoelectrochemical processes at n-GaAs (100)/aqueous HCl electrolyte interface: a synchrotron photoemission spectroscopy study of emersed electrodes, J. Phys. Chem. C 118 (2014) 12774–12781, https://doi.org/10.1021/jp500564c.

[26] S. Nemšák, A. Shavorskiy, O. Karslioglu, I. Zegkinoglou, A Rattanachata, C. S. Conlon, A. K. Keqi, P. Greene, E. C. Burks, F. Salmassi, E. M. Gullikson, S.-H. Yang, K. Liu, H. Bluhm, C. S. Fadley, Concentration and chemical-state profiles at heterogeneous interfaces with sub-nm accuracy from standing-wave ambient-pressure photoemission, Nat. Commun. 5 (2014) 5441, https://doi.org/10.1038/ncomms6441.

[27] S. Axnanda, E. J. Crumlin, B. Mao, S. Rani, R. Chang, P. G. Karlsson, M. O. M. Edwards, M. Lundqvist, R. Moberg, P. Ross, Z. Hussain, Z. Liu, Using "tender" X-ray ambient pressure X-ray photoelectron spectroscopy as a direct probe of solid-liquid interface, Sci. Rep. 5 (2015) 9788, https://doi.org/10.1038/srep09788.

[28] K. Nakanishi, D. Kato, H. Arai, H. Tanida, T. Mori, Y. Orikasa, Y. Uchimoto, T.

Ohta, Z. Ogumi, Novel spectro-electrochemical cell for in situ/operando observation of common composite electrode with liquid electrolyte by X-ray absorption spectroscopy in the tender X-ray region, Rev. Sci. Instrum. 85 (2014) 084103, https://doi.org/10.1063/1.4891036.

[29] J.-J. Velasco-Velez, C. H. Wu, T. A. Pascal, L. F. Wan, J. Guo, D. Prendergast, M. Salmeron, The structure of interfacial water on gold electrodes studied by x-ray absorption spectroscopy, Science 346 (2014) 831-834, https://doi.org/10.1126/science.1259437.

[30] C. H. Wu, T. A. Pascal, A. Baskin, H. Wang, H.-T. Fang, Y.-S. Liu, Y.-H. Lu, J. Guo, D. Prendergast, M. B. Salmeron, Molecular-scale structure of electrode–electrolyte interfaces: the case of platinum in aqueous sulfuric acid, J. Am. Chem. Soc. 140 (2018) 16237-16244, https://doi.org/10.1021/jacs.8b09743.

[31] M. Hattori, K. Yamamoto, M. Matsui, K. Nakanishi, T. Mandai, A. Choudhary, Y. Tateyama, K. Sodeyama, T. Uchiyama, Y. Oikasa, Y. Tamenori, T. Takeguchi, K. Kanamura, Y. Uchimoto, Role of coordination structure of magnesium ions on charge and discharge behavior of magnesium alloy electrode, J. Phys. Chem. C 122 (2018) 25204-25210, https://doi.org/10.1021/acs.jpcc.8b08558.

[32] L. Zhang, D. Sun, J. Kang, H.-T. Wang, S.-H. Hsieh, W.-F. Pong, H. A. Bechtel, J. Feng, L.-W. Wang, E. J. Cairns, J. Guo, Tracking the chemical and structural evolution of the TiS_2 electrode in the lithium-ion cell using operando x-ray absorption spectroscopy, Nano Lett. 18 (2018) 4506-4515, https://doi.org/10.1021/acs.nanolett.8b01680.

[33] M. Nagasaka, H. Yuzawa, T. Horigome, A. P. Hitchcock, N. Kosugi, Electrochemical reaction of aqueous iron sulfate solutions studied by Fe L-edge soft x-ray absorption spectroscopy, J. Phys. Chem. C 117 (2013) 16343–16348, https://doi.org/10.1021/jp405112r.

[34] D. Schön, J. Xiao, Orcid, R, Golnak, M. F. Tesch, B. Winter, J.-J. Velasco-Velez, E. F. Aziz Introducing Ionic-Current Detection for X-ray Absorption Spectroscopy in Liquid Cells, J. Phys. Chem. Lett. 8 (2017) 2087–2092, https://doi.org/10.1021/acs.jpclett.7b00646.

[35] H. P. Hratchian, H. B. Schlegel, Finding minima, transition states, and following reaction pathways on ab initio potential energy surfaces, in C. E. Dykstra, G. Frenking, K. S. Kim, G. E. Scuseria (Eds.), In Theory and Application of Computational Chemistry: The First Forty Years, first ed, Elsevier, New York, 2005, p. 195.

[36] F. Neese, Prediction of molecular properties and molecular spectroscopy with density functional theory: From fundamental theory to exchange-coupling, Coord. Chem. Rev. 253 (2009) 526-563,

https://doi.org/10.1016/j.ccr.2008.05.014.

[37] C. Lee, W. Yang, R. G. Parr, Density-functional exchange-energy approximation with correct asymptotic behavior, Phys. Rev. B 37 (1988) 785.

[38]   F. Weigend, R. Ahlrichs, Balanced basis sets of split valence, triple zeta valence and quadruple zeta valence quality for H to Rn: Design and assessment of accuracy, Phys. Chem. Chem. Phys. 7 (2005) 3297-3305, https://doi.org/10.1039/B508541A.

[39]   S Pathak, L Lang, F Neese, A dynamic correlation dressed complete active space method: Theory, implementation, and preliminary applications, J. Chem. Phys. 147 (2017) 234109, https://doi.org/10.1063/1.5017942.

[40]   B. de Souza, G. Farias, F. Neese, R. Izsak, Predicting phosphorescence rates of light organic molecules using time-dependent density functional theory and the path integral approach to dynamics, Chem. Theory Comput. 15 (2019) 1896-1904, https://doi.org/10.1021/acs.jctc.8b00841.

[41] G. Ren, Y. Ha, Y.-S. Liu, X. Feng, N. Zhang, P. Yu, L. Zhang, W. Yang, J. Feng, J. Guo, X. Liu, Deciphering the Solvent Effect for the Solvation Structure of Ca^{2+} in Polar Molecular Liquids, J. Phys. Chem. B 124 (2020) 3408–3417, https://doi.org/10.1021/acs.jpcb.0c02437.

[42] M. L. Thomas, K. Yamanaka, T. Ohtab, H. R. Byon, perfluorinated moiety-grafted carbon nanotube electrode for the non-aqueous lithium–oxygen battery, Chem. Commun., 51 (2015) 3977-3980, https://doi.org/10.1039/C4CC08815H.

[43] Y. V. Lavskaya, L.G. Bulusheva, A.V. Okotrub, N.F. Yudanov, D.V. Vyalikh, A. Fonseca, Comparative study of fluorinated single-and few-wall carbon nanotubes by X-ray photoelectron and X-ray absorption spectroscopy, Carbon 47 (2009) 1629-1636, https://doi.org/10.1016/j.carbon.2009.01.046.

[44] H. Wang, C. H Wu, R. S. Weatherup, B. Feng, Y. Ye, Y.-S. Liu, P.-A. Glans, J. Guo, H.-T. Fang, M. B. Salmeron, X-ray-induced fragmentation of imidazolium-based ionic liquids studied by soft X-ray absorption spectroscopy, J. Phys. Chem. Lett. 9 (2018) 785−790, https://doi.org/10.1021/acs.jpclett.8b00057.

[45] A. Fujimori, T. Araki, H. Nakahara, E. Ito, M. Hara, H. Ishii, Y. Ouchi, K. Seki, Polarized near edge X-ray absorption fine structure spectroscopic study on organized molecular films of fluorinated comb polymers with various chain lengths, Langmuir 18 (2002) 1437-1440, https://doi.org/10.1021/la011177p.

Author Contributions

⊥L. C. K. and X. F. contributed equally to this work.